MK-Prime-NC-0001-3 core
datasheet

Grid Asset Performance > Next Generation Transformers

The wide tape-wound core is manufactured with Finemet iron-based metal amorphous nanocomposite. Hitachi cast the ribbon material as 8.4” wide ribbon and slit to 3” wide ribbon to eliminate core stacking. MK Magnetics Inc. fabricated and annealed the core with a transverse field for square BH loops. While targeting a 10 kW, 20 kHz three-port active bridge application, this core material can generally be used for transformers, pulse power cores, motors, and high frequency inductors. The 0001 and 3 in the name specify the 0.001 inch thickness and 3 inch ribbon width, respectively.

Date: June 2019
Revision 0.2

Fig. 1: Core under test.

MK-Prime-NC-0001-3 core

Dimensions

Table 1: Core dimensions.

Description	Value
H	74mm
T	8.5mm
G	57mm
C	16mm
W/2	33mm
W	66mm
D	76.2mm (3 inch)

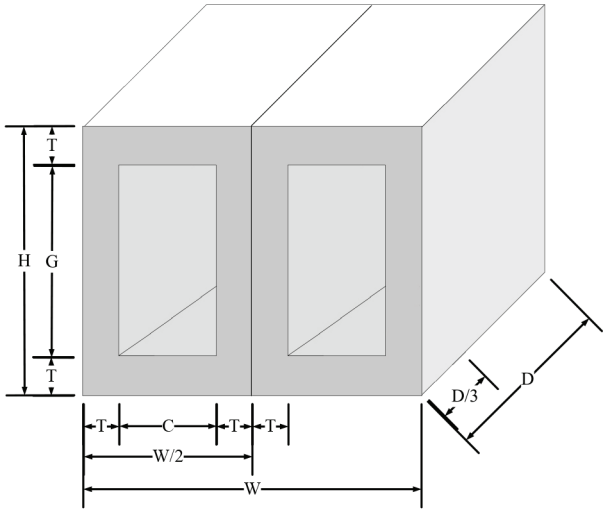

Fig. 2: Illustration of core dimensions.

Acknowledgement

This technical effort was performed in support of the National Energy Technology Laboratory’s ongoing research in DOE’s The Office of Electricity’s (OE) Transformer Resilience and Advanced Components (TRAC) program under the RSS contract 89243318CFE000003.

NATIONAL ENERGY TECHNOLOGY LABORATORY

Magnetic Characteristics

Table 2: Magnetic characteristic.

Description	Symbol	Typical value	Unit
Effective area	A_e	10.152	mm^2
Mean magnetic path length[1]	L_m	168	mm
Mass		1.353	kg

Measurement Setup

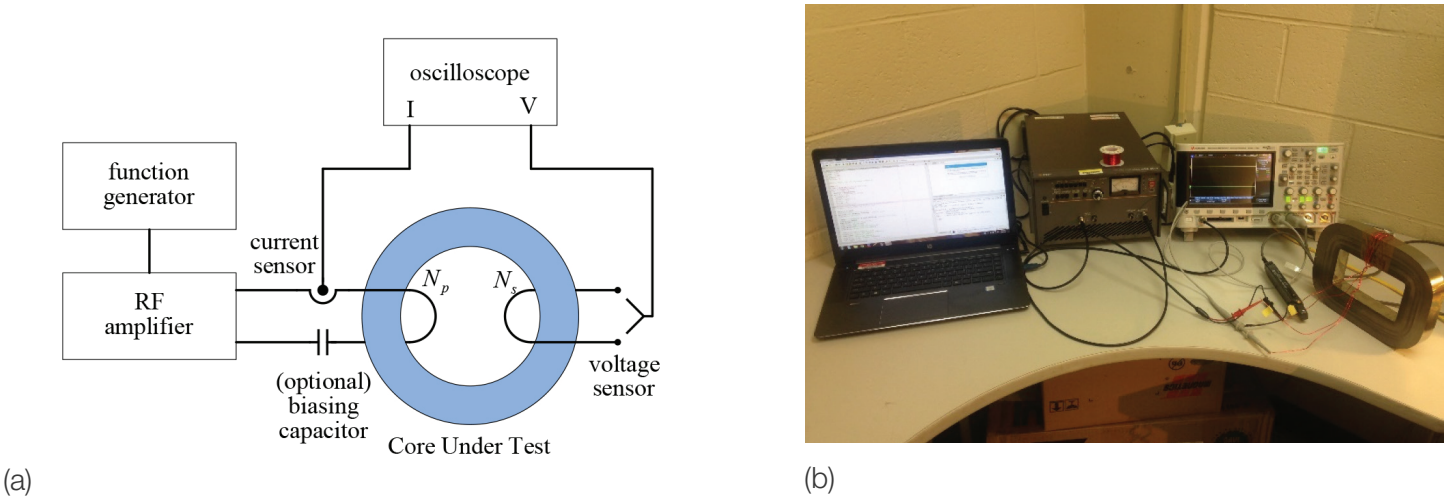

Fig. 3: Arbitrary waveform core loss test system (CLTS) (a) conceptual setup (b) actual setup.

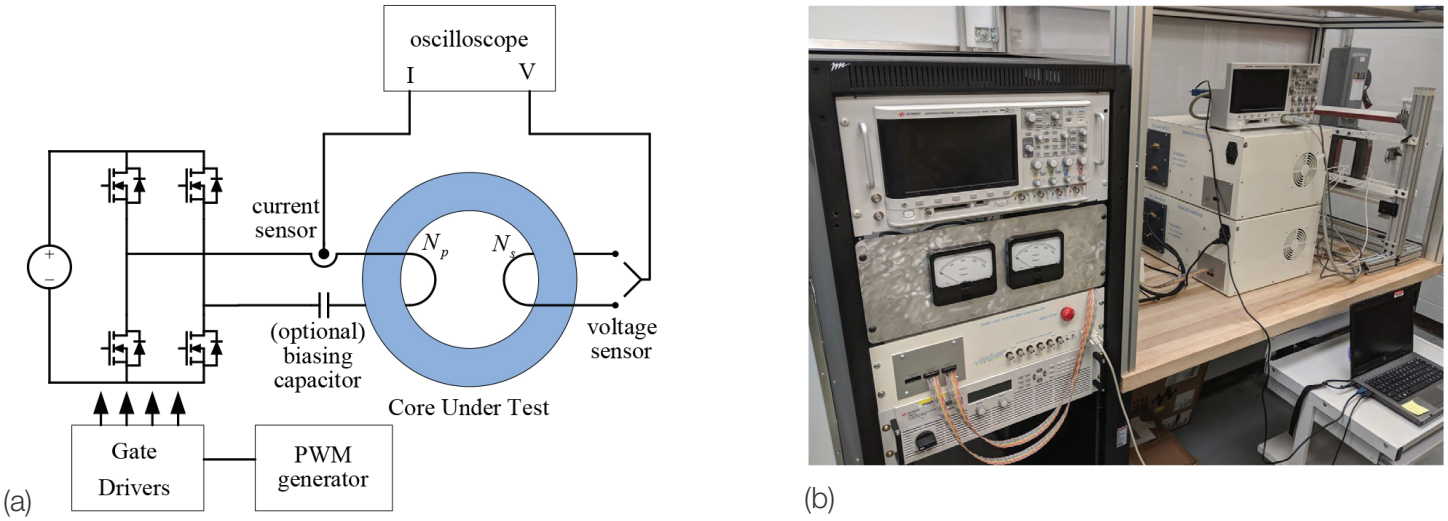

Fig. 4: Square waveform core loss test system (CLTS) (a) conceptual setup (b) actual setup.

[1] Mean magnetic path length is computed using the following equation. OD and ID are outer and inner diameters, respectively. $L_m = \dfrac{\pi(\mathrm{OD}-\mathrm{ID})}{\ln\left(\dfrac{\mathrm{OD}}{\mathrm{ID}}\right)}$

Arbitrary and square waveform core loss test systems (CLTS) are utilized to characterize soft magnetic materials, which are shown in Fig. 3 and Fig. 4, respectively. Fig. 5 illustrates three different excitation voltage waveforms and corresponding flux density waveforms. In the arbitrary waveform CLTS, a function generator generates any arbitrary small signal, and the small signal is amplified and applied to a core under test (CUT) using a linear amplifier. The arbitrary waveform CLTS is advantageous in that any waveforms can be easily applied to characterize a CUT; however, the linear amplifier has limited electrical capabilities, such as ±75V & ±6A peak ratings and 400V/μs slew rate. Therefore, a full core characterization may not be possible in some cases, such as low permeability cores, high frequency, and/or large sized cores. The arbitrary waveform CLTS is utilized to perform sinusoidal waveform measurements, as shown in Fig. 5(a). The square waveform CLTS is utilized to perform various square waveform measurements with different duty cycles, as shown in Fig. 5(b) and (c). 1200V SiC MOSFET devices are utilized to extend the core characterization range.

Two windings are placed around the core under test. The amplifier excites the primary winding, and the current of the primary winding is measured, in which the current information is converted to the magnetic field strengths H as

$$H(t) = \frac{N_p \cdot i(t)}{l_m}, \qquad (1)$$

where N_p is the number of turns in the primary winding. A dc-biasing capacitor is inserted in series with the primary winding to provide zero average voltage applied to the primary winding.

The secondary winding is open, the voltage across the secondary winding is measured, in which the voltage information is integrated to derive the flux density B as

$$B(t) = \frac{1}{N_s \cdot A_e} \int_0^T v(\tau)\, d\tau, \qquad (2)$$

where N_s is the number of turns in the secondary winding, and T is the period of the excitation waveform.

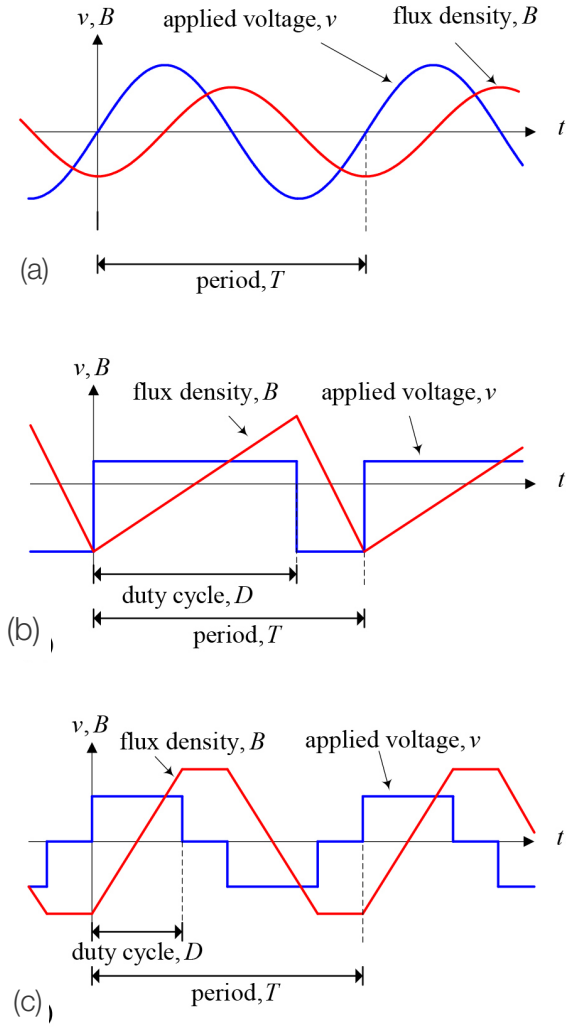

Fig. 5: Excitation voltage waveforms and corresponding flux density waveforms (a) Sinusoidal excitation with sinusoidal flux, (b) Asymmetrical excitation with sawtooth flux, and (c) Symmetrical excitation with trapezoidal flux.

In Fig. 5(a), the excitation voltage is sinusoidal, and its flux waveform is also a sinusoidal shape. In Fig. 5(b), the excitation voltage is a two-level square waveform with asymmetrical duty cycle between high-level and low-level voltages, and its flux waveform is a sawtooth shape. It is hereafter referred as asymmetrical waveform. Its duty cycle is defined as the ratio between the applied high voltage time and the period, and the duty cycle can range from 0% to 100%. Furthermore, the average excitation voltage is adjusted to be zero via the dc-biasing capacitor, and thus, the average flux is also zero. In Fig. 5 (c), the excitation voltage is a three-level square voltage with symmetrical duty cycle between high-level and low-level voltages, and its flux waveform is a trapezoidal shape. It is hereafter referred as symmetrical waveforms. Its duty cycle is defined as the ratio between the applied high-level voltage time and the period, and the duty cycle can range from 0% to 50%. At 50% duty cycles, both the asymmetrical and symmetrical waveforms become identical.

Core Losses

Core losses at various frequencies and induction levels are measured using various excitation waveforms. Based on measurements, the coefficients of the Steinmetz's equation are estimated. The Steinmetz's equation is given as

$$P_w = k_w \cdot \left(f / f_0 \right)^{\alpha} \cdot \left(B / B_0 \right)^{\beta} , \tag{3}$$

where P_w is the core loss per unit weight, f_0 is the base frequency, B_0 is the base flux density, and k_w, α, and β are the Steinmetz coefficients from empirical data. In the computation of P_w, the weight before impregnation in Table 2 is used, the base frequency f_0 is 1 Hz, and the base flux density B_0 is 1 Tesla.

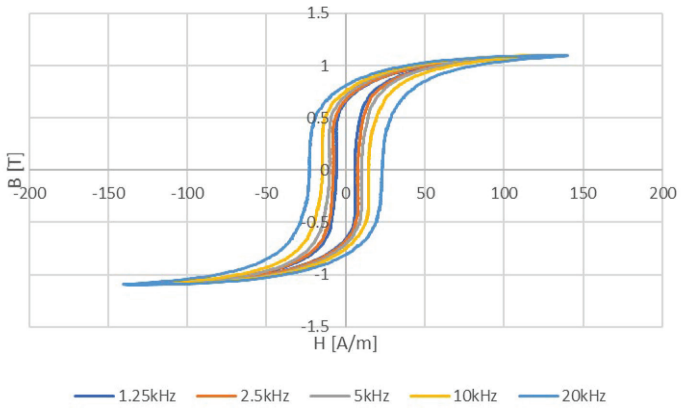

Fig. 6: BH curve as a function of frequency.

Fig. 6 illustrates the measured BH curve at different frequencies. The field strength H is kept near constant for all frequency. At 1.25 kHz and 2.5 kHz excitations, the BH curve is similar, which indicates that the hysteretic losses are the dominant factor at frequencies below 1.25 kHz. As frequency increases, the BH curves become thicker, which indicates that the eddy current and anomalous losses are becoming larger.

Table 3: Empirical Steinmetz coefficients.

	k_w	A	β
sine	6.63921346590435e-05	1.56467873348185	1.91259697460311
Square 50% duty	3.14818429983634e-05	1.58482167338229	1.94903512891532
Asymmetrical 40% duty	3.02461044734152e-05	1.59109424199687	2.04041874955223
Asymmetrical 30% duty	2.97352171515145e-05	1.60355723729451	2.09603243106937
Asymmetrical 20% duty	3.39730988963156e-05	1.63816739427575	2.62829182277307
Asymmetrical 10% duty	2.14514168122723e-05	1.77465534082535	2.33182525022425
Symmetrical 40% duty	1.11179776869807e-05	1.77724707022187	2.44728918939305
Symmetrical 30% duty	1.01177492927937e-05	1.80932305941750	2.42436011613974
Symmetrical 20% duty	1.15769129008774e-05	1.83004940930183	2.34791603110533
Symmetrical 10% duty	1.32794674715137e-05	1.87453610313042	2.22712627028489

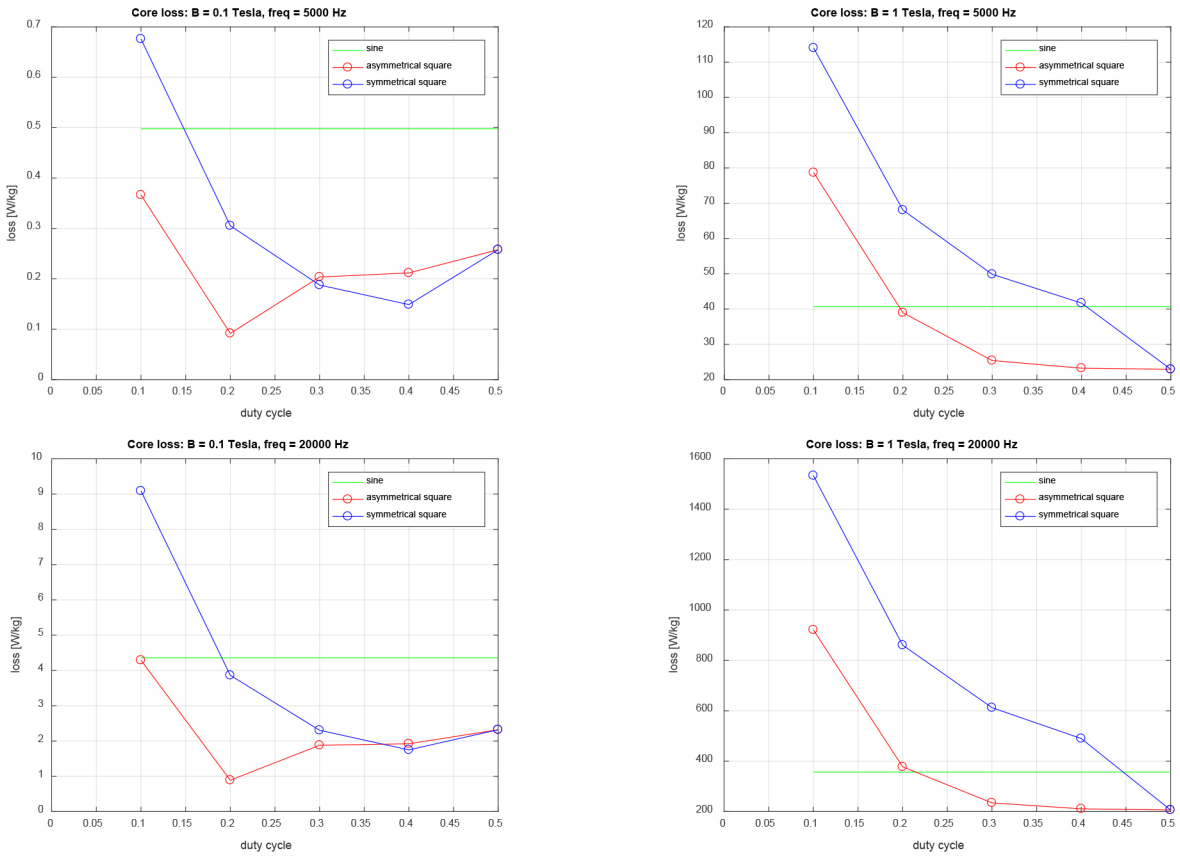

Fig. 7: Estimated core losses of sine and square excitation at various flux density, frequency, and duty cycle.

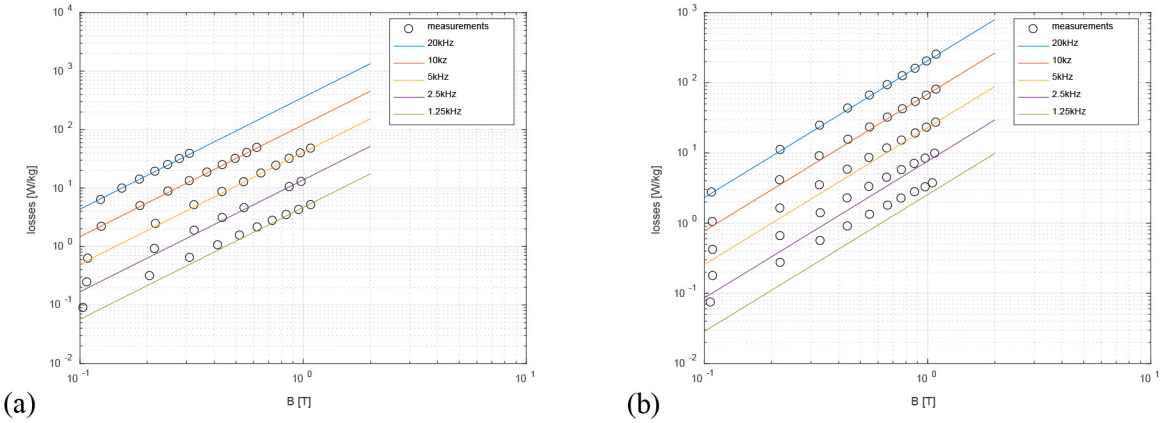

Fig. 8: Core loss measurements and estimations via Steinmetz equation: (a) Sine (b) Square at 50% duty.

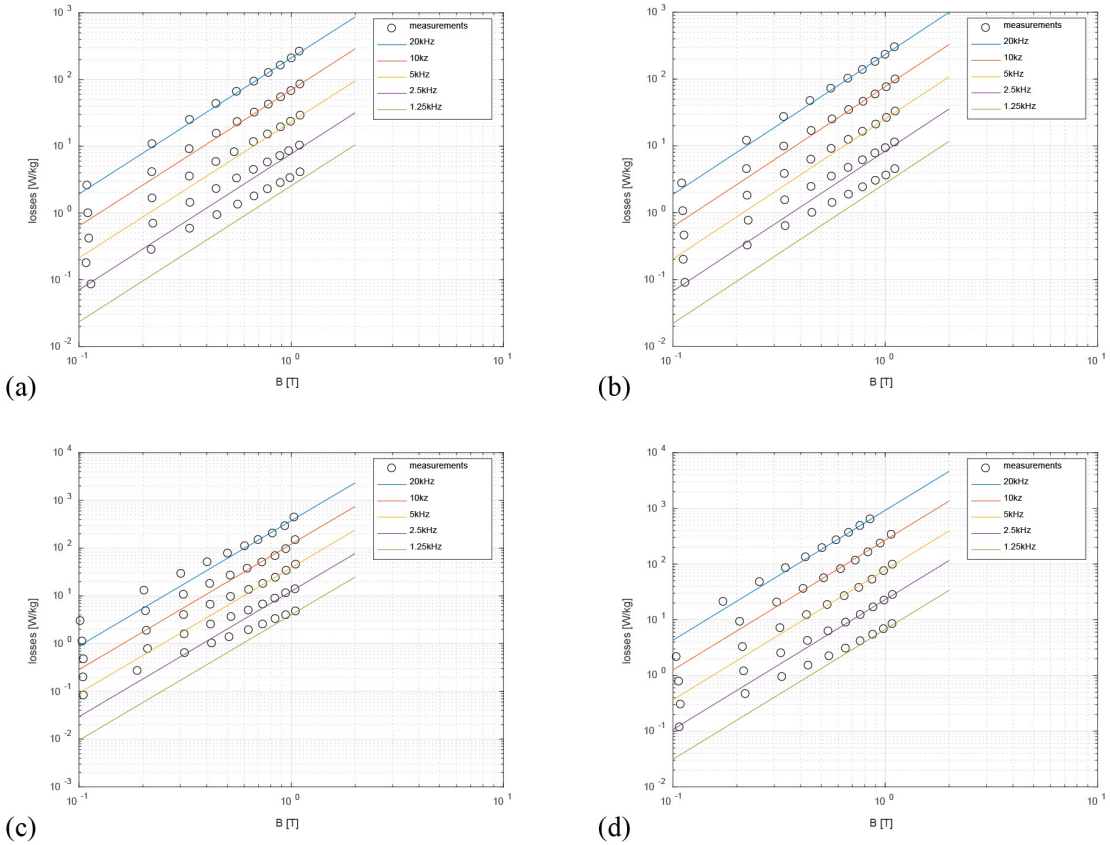

Fig. 9: Core loss measurements and estimations via Steinmetz equation of asymmetrical square waveform excitation: (a) 40% duty (b) 30% duty (c) 20% duty (d) 10% duty.

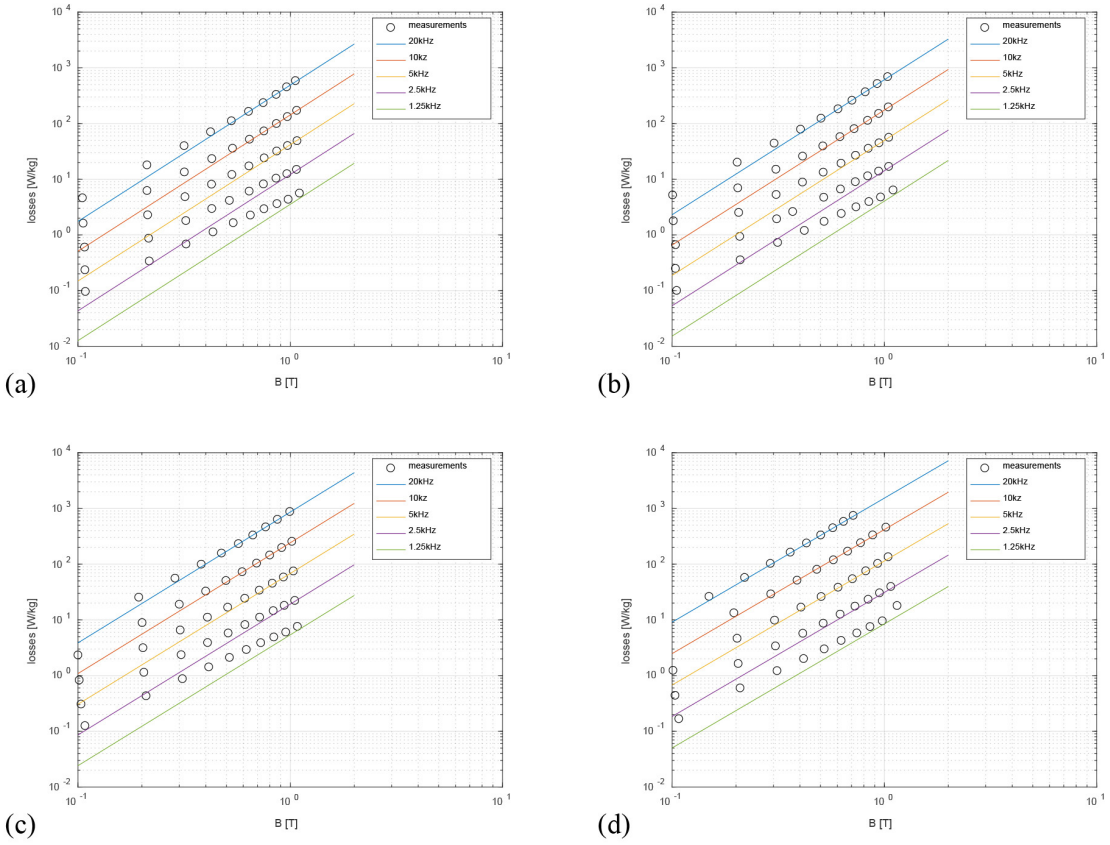

Fig. 10: Core loss measurements and estimations via Steinmetz equation of symmetrical square waveform excitation: (a) 40% duty (b) 30% duty (c) 20% duty (d) 10% duty.

Table 3 lists the Steinmetz coefficients at different excitation conditions.

Fig. 7 illustrates estimated core losses of sine and square excitation at various flux density, frequency, and duty cycle based on the empirical Steinmetz coefficients in Table 3.

Fig. 8, Fig. 9, and Fig. 10 illustrate the core loss measurements data points and estimations via Steinmetz equation of sine, asymmetrical, and symmetrical square excitation waveforms at various duty cycles.

Core Permeability

The permeability of the core is measured as functions of flux density and frequency. Following figures illustrate the measured absolute relative permeability μ_r values, which is defined as

$$\mu_r = \frac{B_{peak}}{\mu_0 \cdot H_{peak}} \tag{4}$$

where B_{peak} and H_{peak} are the maximum flux density and field strength at each measurement point. Under certain excitation conditions, the core could not be saturated due to lack of available voltages. For example, the sine excitation is performed using the arbitrary CLTS, and its voltage is limited to ±75V. Furthermore, the square CLTS could not saturate the core during the highest frequency and 10% duty cycle.

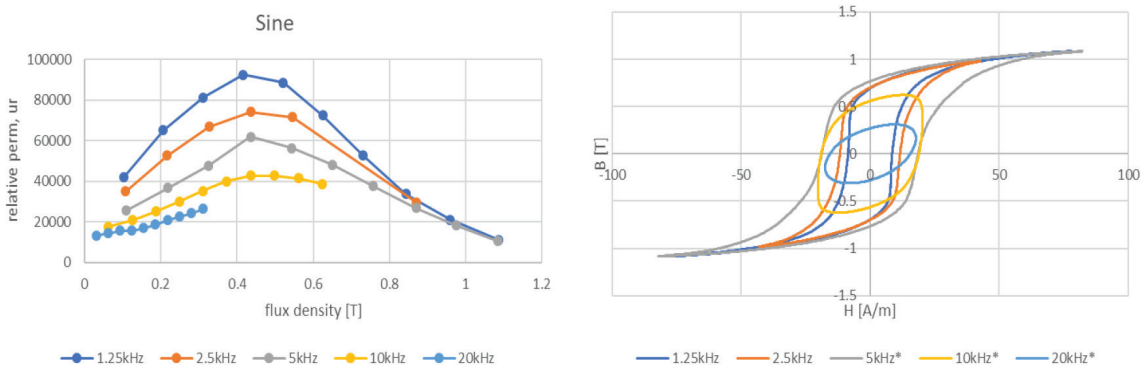

Fig. 11 Sinusoidal excitation: relative permeability as a function of flux density and frequency (left column) and BH loop at the maximum B of the corresponding frequency (right column).

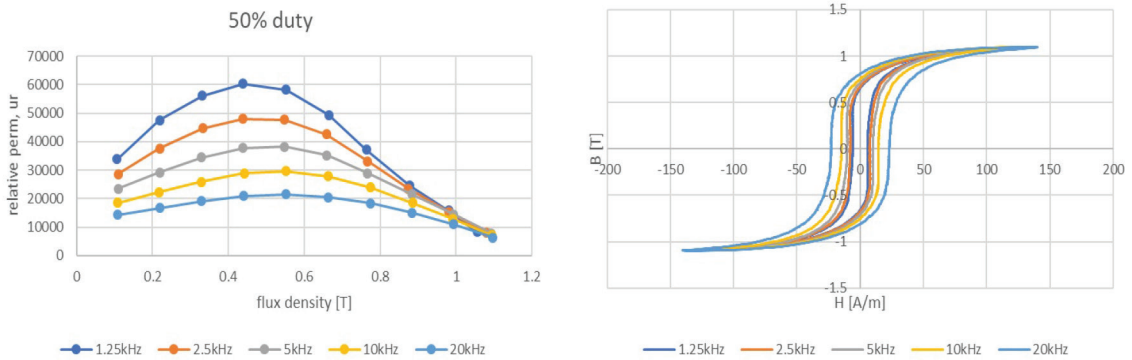

Fig. 12: Square excitation with 50% duty cycle: relative permeability as a function of flux density and frequency (left column) and BH loop at the maximum B of the corresponding frequency (right column).

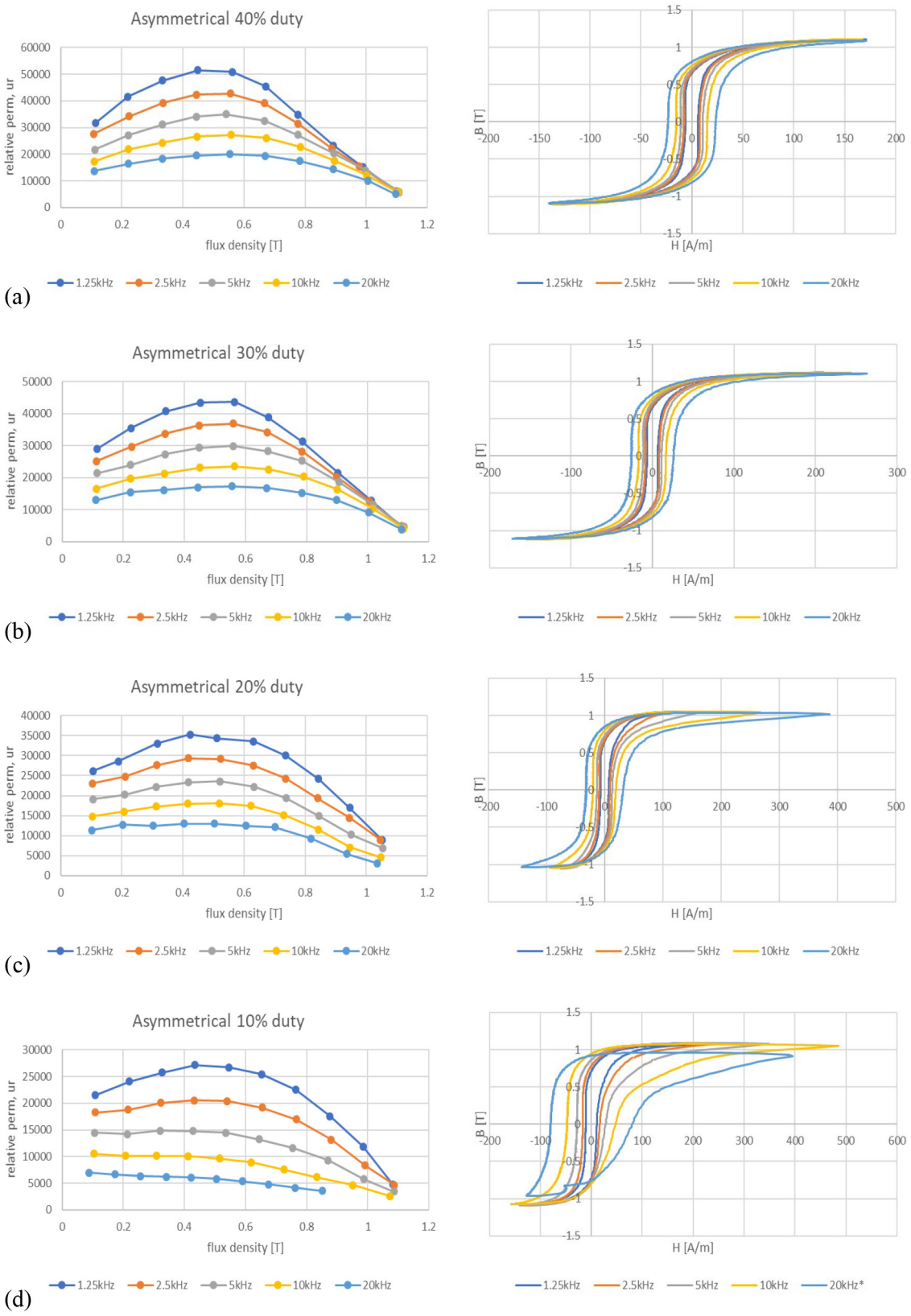

Fig. 13: Asymmetrical excitation with various duty cycle: relative permeability as a function of flux density and frequency (left column) and BH loop at the maximum B of the corresponding frequency (right column) (a) 40% duty (b) 30% duty (c) 20% duty (d) 10% duty.

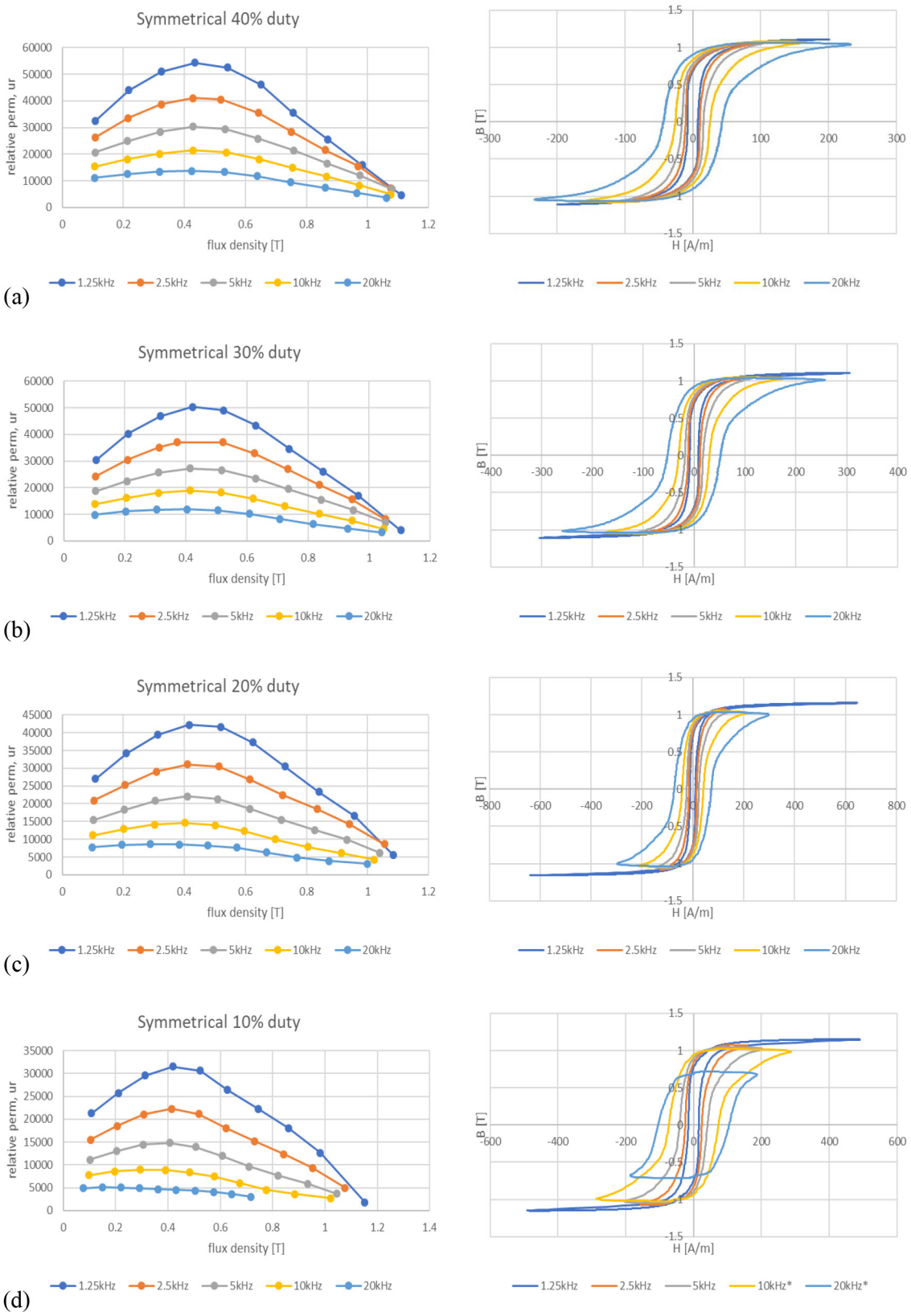

Fig. 14: Symmetrical excitation with various duty cycle: relative permeability as a function of flux density and frequency (left column) and BH loop at the maximum B of the corresponding frequency (right column) (a) 40% duty (b) 30% duty (c) 20% duty (d) 10% duty (could not saturate the core under the condition).*

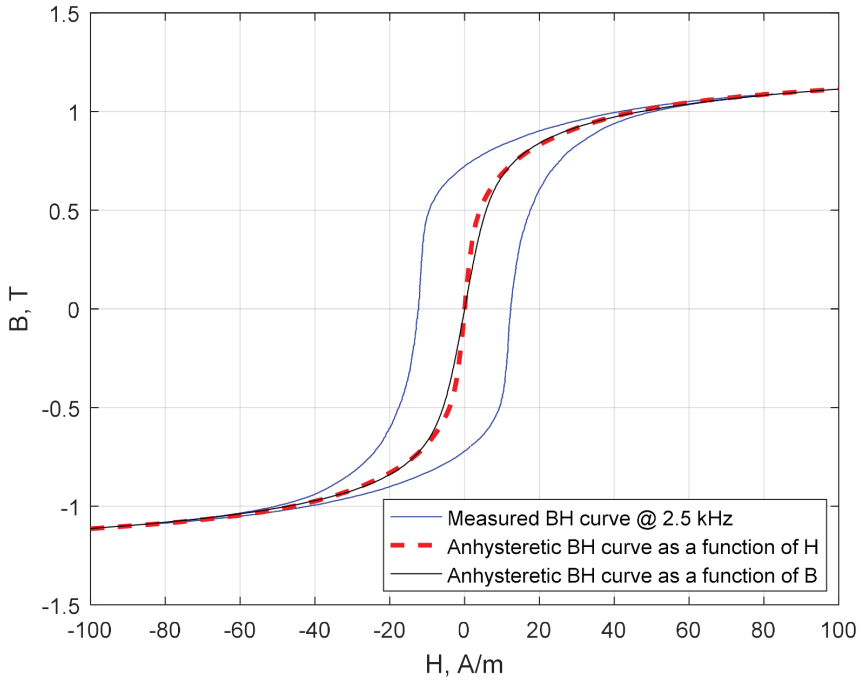

Fig. 15: Measured BH curve and fitted anhysteretic BH curve as functions of H and B.

Table 4: Anhysteretic curve coefficients for B as a function of H.

k	1	2	3	4
m_k	1.46959155768125	0.241510135103053	-0.392157054276167	-0.211747731733556
h_k	9.59306407150722	3.26684630353795	96.8643663782641	26.9714974683604
n_k	1	2.41644289279169	1.59506808211518	2.41781082297097

Table 5: Anhysteretic curve coefficients for H as a function of B.

k	1	2	3	4
μ_r	82811.4222458864			
α_k	0.588300138552808	0.0162366198182290	0.0162321970090029	0.0155581999897635
β_k	63.9078805757331	5.69495105813105	14.1785921854897	61.6235789814661
γ_k	1.45850055621626	1.73240545548081	1.40442879578233	1.37721461288524
δ_k	0.00920543966179025	0.00285105519827900	0.00114483841531283	0.000252471541687685
ε_k	3.30788643594443e-41	5.19091131699811e-05	2.24890332378490e-09	1.38646170975675e-37
ζ_k	1	0.999948090886830	0.999999997751097	1

Fig. 15 illustrates the measured BH curve and fitted anhysteretic BH curves as functions of H and B using the coefficients from Table 4 and Table 5. Fig. 16 and Fig. 17 illustrates the absolute relative permeability as functions of field strength H and flux density B, respectively. Fig. 18 illustrates the incremental relative permeability.

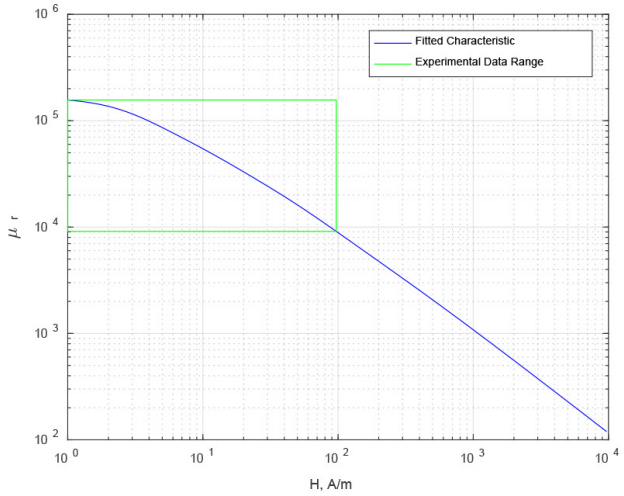

Fig. 16: Absolute relative permeability as function of field strength H.

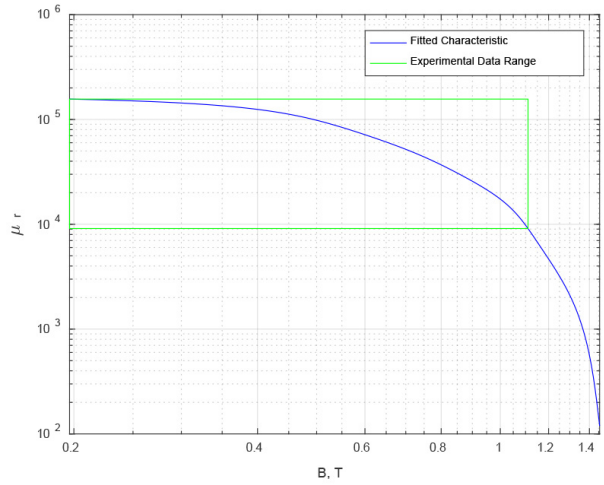

Fig. 17: Absolute relative permeability as function of flux density B.

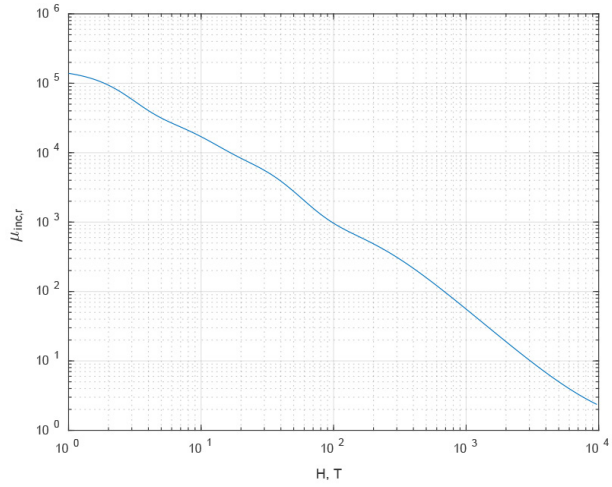

Fig. 18: Incremental relative permeability.

Fig. 15 illustrates the measured BH curve and fitted anhysteretic BH curves as functions of H and B. The anhysteretic BH curves can be computed as a function of field intensity H using the following formula.

$$B = \mu_H(H)H$$
$$\mu_H(H) = \mu_0 + \sum_{k=1}^{K} \frac{m_k}{h_k} \frac{1}{1+\left|H/h_k\right|^{n_k}} \tag{5}$$

Similarly, the anhysteretic BH curves can be computed as a function of flux density B using the following formula.

$$B = \mu_B(B)H$$
$$\mu_B(B) = \mu_0 \frac{r(B)}{r(B)-1}$$
$$r(B) = \frac{\mu_r}{\mu_r - 1} + \sum_{k=1}^{K} \alpha_k |B| + \delta_k \ln\left(\varepsilon_k + \zeta_k e^{-\beta_k |B|}\right) \tag{6}$$
$$\delta_k = \frac{\alpha_k}{\beta_k}, \varepsilon_k = \frac{e^{-\beta_k \gamma_k}}{1+e^{-\beta_k \gamma_k}}, \zeta_k = \frac{1}{1+e^{-\beta_k \gamma_k}}$$

Table 4 and Table 5 lists the anhysteretic curve coefficients for eqs. (5) and (6), respectively.

Fig. 16 and Fig. 17 illustrates the absolute relative permeability as functions of field strength H and flux density B, respectively. Fig. 18 illustrates the incremental relative permeability.

The core anhysteretic characteristic models in eqs. (5) and (6) are based on the following references.

Scott D. Sudhoff, "Magnetics and Magnetic Equivalent Circuits," in *Power Magnetic Devices: A Multi-Objective Design Approach*, 1, Wiley-IEEE Press, 2014, pp.488-

G. M. Shane and S. D. Sudhoff, "Refinements in Anhysteretic Characterization and Permeability Modeling," in *IEEE Transactions on Magnetics*, vol. 46, no. 11, pp. 3834-3843, Nov. 2010.

The estimation of the anhysteretic characteristic is performed using a genetic optimization program, which can be found in the following websites:

https://engineering.purdue.edu/ECE/Research/Areas/PEDS/go_system_engineering_toolbox

Core Characteristic Variation as a Function of Temperature

At this time, the core temperature is not monitored, and this version of data sheet does not have this information. However, in future editions, it is planned to be included.